

Supplementary Information

Design and characterization of visible-light LED sources for microstructured photoreactors

Anca Roibu^a, Rishi Bharadwaj Morthala^a, M. Enis Leblebici^a, Dorota Koziej^b, Tom Van Gerven^a & Simon Kuhn^{*a}

^aKU Leuven, Department of Chemical Engineering, Celestijnenlaan 200F, 3001 Leuven, Belgium.

^bETH Zürich, Laboratory for Multifunctional Materials, Department of Materials, Vladimir-Prelog-Weg 1-5/10, 8093 Zürich, Switzerland. Present address: University of Hamburg, Center for Hybrid Nanostructures (CHyN)

*Correspondence to S.K. (email: simon.kuhn@kuleuven.be)

1. Chemical actinometry and calculation of the photon flux

The photon flux received by the reactor channel was experimentally determined using chemical actinometry. The actinometric measurements were realized using the photoisomerization reaction of the diarylethene derivative, 1,2-bis(2,4-dimethyl-5-phenyl-3-thienyl)perfluorocyclopentene, from its closed (DAE CF) to the open form (DAE OF) in hexane. The initial concentration of DAE CF varied between $7 \cdot 10^{-4}$ M and $8 \cdot 10^{-4}$ M. The experimental procedure is described in detail in our previously reported work¹. The actinometric measurements were conducted at liquid flow rates of 5, 8, 10 and 12 mL min⁻¹ which correspond to residence times of 6.6, 4.1, 3.3 and 2.7 s. At these residence times the conversion of DAE CF was predominantly below 10%. Figure S1.1a illustrates the variation of DAE CF concentration in function of residence time when the reactor was irradiated by the CC-8mm LED array placed at $D = 2$ cm and driven at $I_F = 8$ mA/LED. Lower flow rates, such as 1 and 3 mL min⁻¹, were used when the irradiance on the reactor was too low to determine a quantifiable conversion.

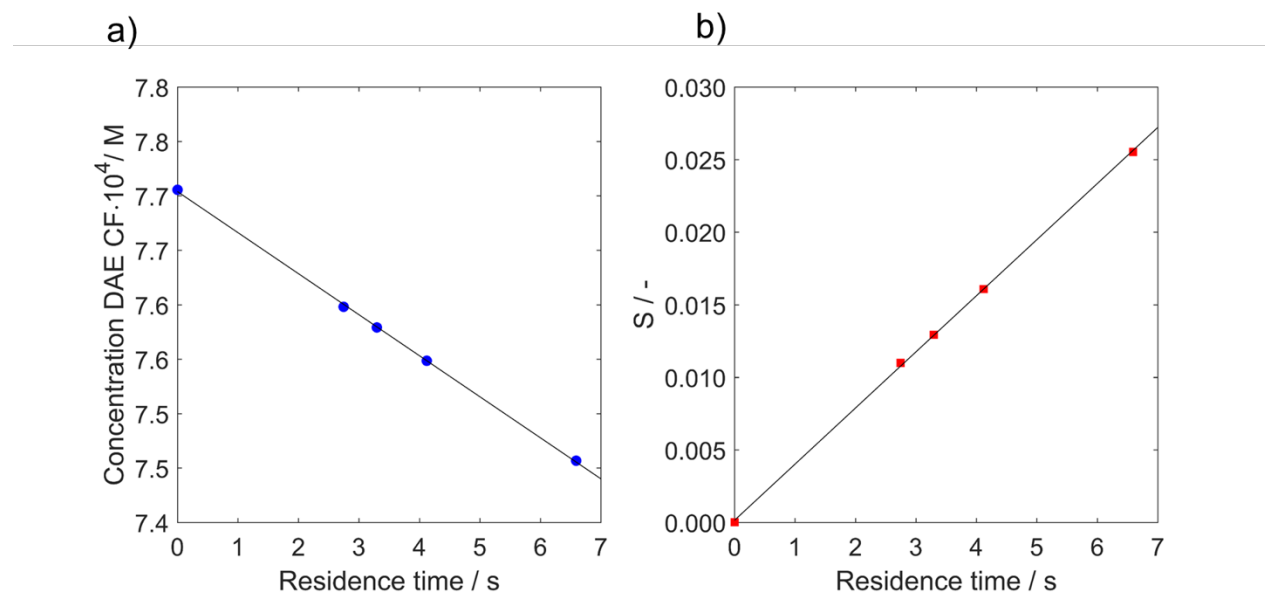


Figure S1.1. a) Variation of DAE CF concentration in function of the residence time, t . b) Variation of S in function of the residence time, t . The experimental results are shown for the CC-8mm, $D = 2$ cm, $I_F = 8$ mA/LED.

The photon flux received in the microreactor channel, I_0 , was calculated using the following equation¹:

$$\underbrace{\log\left(10^{\varepsilon_{\text{avg}}c(0)l_{\text{reactor}}} - 1\right) - \log\left(10^{\varepsilon_{\text{avg}}c(t)l_{\text{reactor}}} - 1\right)}_S = \varepsilon_{\text{avg}} l_{\text{reactor}} \phi_{\text{avg}} \frac{I_0}{V} t \quad (\text{S } 1)$$

where ε_{avg} is the average molar absorption coefficient [M⁻¹cm⁻¹], $c(0)$ is the initial concentration of DAE CF solution [M], $c(t)$ is the final concentration of DAE CF solution [M], l_{reactor} is the

average optical pathlength in the reactor channel ($l_{\text{reactor}} = 0.082 \text{ cm}$ as determined previously¹). ϕ_{avg} is the average quantum yield [mol Einstein^{-1}], I_0 is the photon flux received by the reactor channel [Einstein s^{-1}], V is the irradiated volume [L] which is considered equal to the reactor volume and t is the residence time in the reactor [s].

Figure S1.1b shows the linear variation of S in function of the residence time. The photon flux, I_0 , was determined from the slope of the fitted linear regression as:

$$I_0 = V \frac{\text{slope}}{\varepsilon_{\text{avg}} \phi_{\text{avg}} l_{\text{reactor}}} \quad (\text{S } 2)$$

The average molar absorption coefficient, ε_{avg} , is calculated at each forward current as follows:

$$\varepsilon_{\text{avg}} = \sum_{\lambda=480}^{620} \varepsilon_{\lambda} g_{\lambda} \quad (\text{S } 3)$$

where g_{λ} is the energy density distribution function of the LED light source. g_{λ} was determined as:

$$g_{\lambda} = \frac{E_{\lambda}}{\sum_{\lambda=480}^{620} E_{\lambda}} \quad (\text{S } 4)$$

where E_{λ} is the spectral irradiance of the LED light source [W cm^{-2}] at a certain I_F .

ε_{avg} was calculated for different forward currents, I_F , ranging from 2 to 13 mA (see Fig. S1.2). The obtained values were fitted with a polynomial regression. Therefore, ε_{avg} at any I_F between 2 and 13 mA was obtained using the following fitted polynomial:

$$\varepsilon_{\text{avg}} = -0.1306I_F^3 + 4.456I_F^2 - 63.771I_F + 8762.6 \quad (\text{S } 5)$$

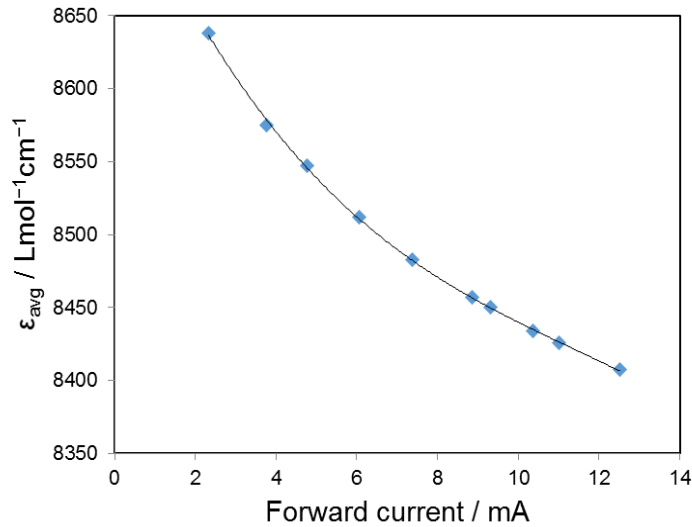


Figure S1.2. Variation of average molar absorption coefficient, ε_{avg} , in function of the forward current, I_F .

The average quantum yield of the photoisomerization from DAE CF to the DAE OF, ϕ_{avg} , is calculated for each forward current as:

$$\phi_{\text{avg}} = \sum_{\lambda=480}^{620} \phi_{\lambda} g_{\lambda} \quad (\text{S } 6)$$

ϕ_{avg} was calculated for different forward currents, I_F , between 2 and 13 mA (see Fig. S1.3) and the obtained values were fitted with a polynomial regression. ϕ_{avg} at any I_F between 2 and 13 mA was obtained using the following equation:

$$\phi_{\text{avg}} = -2 \cdot 10^{-5} I_F^4 + 7 \cdot 10^{-4} I_F^3 - 10^{-2} I_F^2 + 9 \cdot 10^{-2} I_F + 20.9 \quad (\text{S } 7)$$

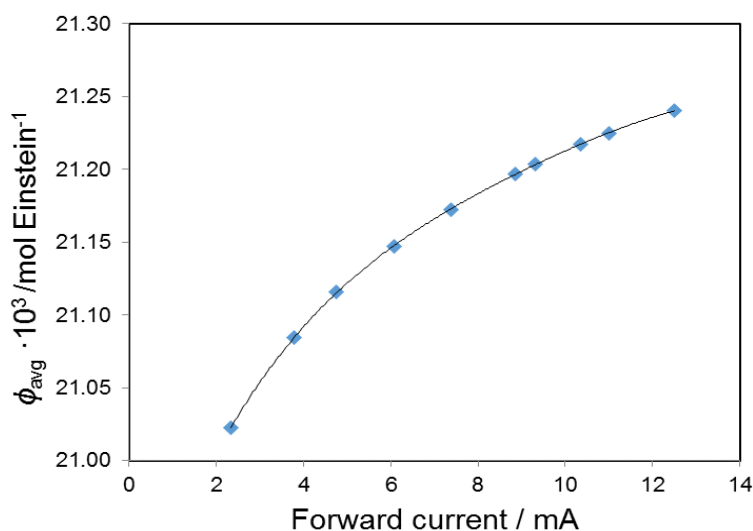


Figure S1.3. Variation of the average quantum yield, ϕ_{avg} , in function of the forward current, I_F .

S2. Influence of irradiance uniformity on actinometric measurements

In this section we evaluate the influence of the light uniformity on the actinometric measurements. As shown in the manuscript, the irradiance uniformity on the reactor channel irradiated by the CC-8mm LED array is 80% at $D = 0.5$ cm and 91% at $D = 2$ cm. At both distances, the variation of the measured photon flux was found to be linear with the forward current, with R^2 values of 0.998 at 0.5 cm and 0.999 at 2 cm. Therefore, it can be concluded that the lower uniformity at 0.5 cm does not affect the results of the actinometric measurements, which could be explained by the fact that the actinometric measurements were performed at low DAE CF conversions (<10%).

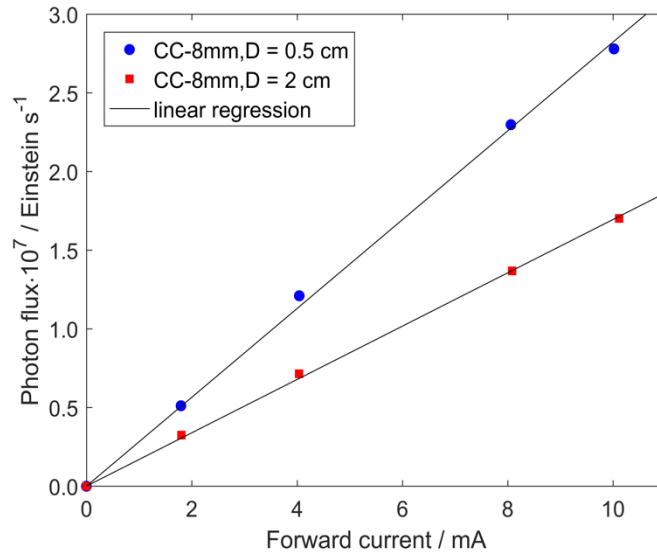


Figure S2. Variation of the photon flux, I_0 , in function of the forward current, I_F , at $D = 0.5$ cm and $D = 2$ cm.

S3. Calculation of the radiant flux

The conversion from the photon flux received in the reactor to the radiant flux was realized as follows:

$$\Phi_{\text{reactor}} = I_0 N_A E_{\text{photon,avg}} \quad (\text{S } 8)$$

where Φ_{reactor} is the radiant flux received in the reactor channel [W], N_A is Avogadro's number ($6.02214 \cdot 10^{23} \text{ mol}^{-1}$). $E_{\text{photon,avg}}$ is the averaged energy of the emitted photons [J] which was calculated as:

$$E_{\text{photon,avg}} = \sum_{\lambda=480}^{620} E_{\text{photon},\lambda} g_{\lambda} \quad (\text{S } 9)$$

where $E_{\text{photon},\lambda}$ is the energy carried by a photon with the wavelength, λ . $E_{\text{photon},\lambda}$ is equal to:

$$E_{\text{photon},\lambda} = \frac{hc}{\lambda} \quad (\text{S } 10)$$

where h is Planck's constant ($6.62607 \cdot 10^{-34} \text{ J s}$) and c is the speed of light equal to $2.998 \cdot 10^8 \text{ m s}^{-1}$.

$E_{\text{photon,avg}}$ was calculated for different forward currents, I_F , between 2 and 13 mA (see Fig. S3) and the obtained values were fitted with a polynomial regression. $E_{\text{photon,avg}}$ at any I_F between 2 and 13 mA was obtained using the following equation:

$$E_{\text{photon,avg}} = 3 \cdot 10^{-6} I_F^5 - 10^{-4} I_F^4 + 2 \cdot 10^{-3} I_F^3 - 1.78 \cdot 10^{-2} I_F^2 + 10^{-1} I_F + 37.299 \quad (\text{S } 11)$$

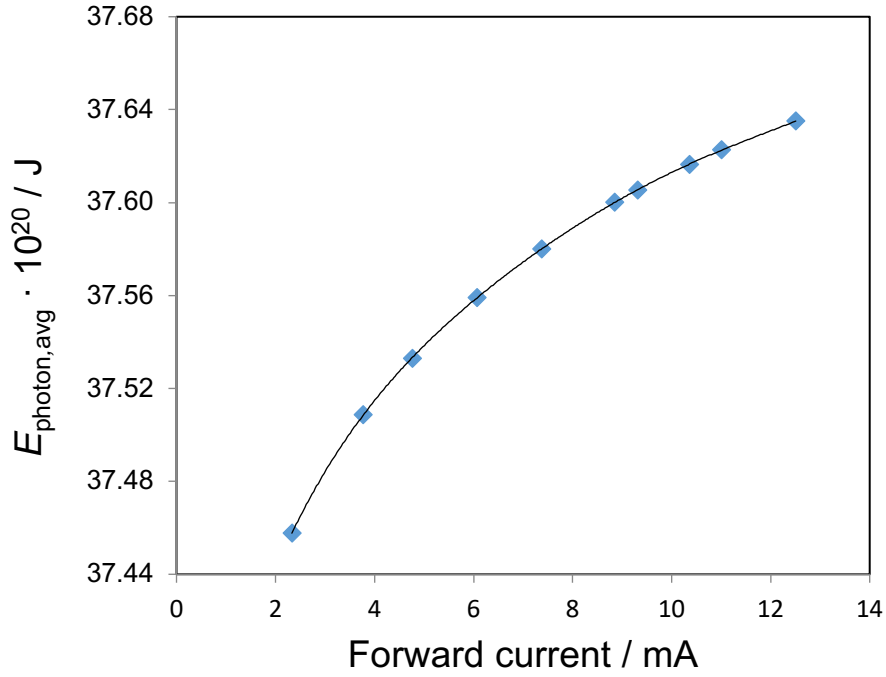


Figure S3. Variation of the average photon energy, $E_{\text{photon,avg}}$, in function of the forward current, I_F .

S4. Angular irradiance distributions

The irradiance profiles extracted from the ray tracing software were normalized by the maximum irradiance. The normalized irradiance distributions were fitted by nonlinear regression to a series of 8 Gaussian distributions according to:

$$E(\theta) = \sum_{i=1}^8 a_i e^{-\left(\frac{\theta - b_i}{c_i}\right)^2} \quad (\text{S } 12)$$

where a_i , b_i and c_i are the fitting coefficients and θ is the polar angle [rad]. The fitting was performed using the *Curve fitting toolbox* in Matlab.

In this work the irradiance distribution at different distances, D , were modelled using the coefficients listed in Table S4.

Table S4. Equation coefficients for modeling the angular irradiance distribution at different distances, D .

Coefficients	D = 0.1 cm	D = 0.5 cm	D = 1 cm	D = 1.5 cm	D = 2 cm
a1	0.09158	0.3481	0.2836	0.04294	0.02066
b1	-0.7191	0.04859	0.0239	0.03517	0.04803
c1	0.1917	0.09251	0.07544	0.04402	0.02308
a2	0.512	0.06036	0.01525	0.7382	0.01544
b2	-0.4745	0.1159	-0.03449	-0.1034	-0.0663
c2	0.05676	0.04261	0.0439	0.1501	0.02432
a3	0.4258	0.609	0.3043	0.7246	0.6414
b3	-0.3179	-0.05539	0.08024	0.1152	0.08883
c3	0.1886	0.1321	0.07201	0.1402	0.1083
a4	0.4535	0.5244	0.7867	0.1128	0.03518
b4	-0.02106	-0.2253	-0.1062	0.01786	0.005598
c4	0.336	0.1268	0.1593	0.637	0.02843
a5	0.5405	0.6383	0.4715	0.4706	0.7516
b5	0.06385	0.1946	0.1583	-0.2905	-0.08218
c5	0.3185	0.1262	0.08236	0.1044	0.1336
a6	0.3195	0.5287	0.1032	0.05046	0.6033
b6	0.3439	0.3692	0.02164	-0.3901	0.2565
c6	0.1765	0.08536	0.6923	0.02872	0.1249
a7	0.4852	0.4723	0.6208	0.4552	0.552
b7	0.4795	-0.3733	0.2971	0.2964	-0.2687
c7	0.05311	0.08428	0.1128	0.09935	0.1195
a8	0.08913	0.1378	0.4835	0.05211	0.09013
b8	0.7359	0.01721	-0.3147	0.4024	0.016
c8	0.2352	0.702	0.1074	0.02039	0.6686

Table S4. (continued) Equation coefficients for modeling the angular irradiance distribution at different distances, D .

Coefficients	D = 2.5 cm	D = 3 cm	D = 3.5 cm	D = 4 cm	DS
a1	0.31	0.02881	0.2748	0.02691	0.03796
b1	0.0545	-0.6627	0.08297	0.0976	-0.1401
c1	0.04631	0.1909	0.08747	0.03215	2.716
a2	0.1907	0.02307	0.3527	0.6341	0.02571
b2	0.005083	-0.5399	-0.2636	-0.08001	-0.5991
c2	0.05741	0.06736	0.1055	0.1073	0.1566
a3	0.4279	0.7618	0.07889	0.623	0.8449
b3	0.1124	-0.2203	0.01055	0.05603	-0.1027
c3	0.0575	0.151	0.6671	0.106	0.1998
a4	0.77	0.8168	0.009104	0.02668	0.4318
b4	-0.06909	0.05365	0.5496	-0.1969	0.07382
c4	0.1261	0.1187	0.03236	0.01622	0.09871
a5	0.5749	0.4006	0.04551	0.6629	0.4352
b5	-0.2554	-0.08064	-0.37	0.2175	0.2368
c5	0.1223	0.08689	0.0218	0.1392	0.1368
a6	-2.545	0.651	0.5609	0.6211	0.0221
b6	0.2538	0.2362	0.2325	-0.2378	0.551
c6	0.09806	0.1355	0.1332	0.1297	0.1875
a7	0.0907	0.01171	0.2619	0.06768	0.059
b7	0.01988	0.5478	-0.08236	0.06615	-0.05071
c7	0.6517	0.04155	0.1398	0.6688	0.0589
a8	3.195	0.03863	0.6069	0.01318	0.1594
b8	0.2499	0.4818	-0.0497	-0.5934	0.1816
c8	0.1049	0.4189	0.2176	0.1466	0.08097

S5. Absolute irradiance modeling for an LED array

The absolute irradiance on a parallel plane irradiated by a LED array can be predicted as follows:

$$E(x, y, z) = \sum_M \frac{z}{\left((x - x_0)^2 + (y - y_0)^2 + z^2 \right)^{\frac{3}{2}}} \frac{\Phi_0 E(\theta)}{2\pi \int_0^{\frac{\pi}{2}} E(\theta) \sin \theta d\theta} \quad (\text{S } 13)$$

where M is the number of LEDs of the investigated array and x_0, y_0 are the coordinates of the LEDs. Φ_0 denotes the radiant flux of one LED, which was calculated by dividing the measured radiant flux (using a near-field goniophotometer calibrated with a spectroradiometer) by the number of LEDs in the array.

In this work, the absolute irradiance was quantified for the CC-8mm and MC-8mm LED arrays (near-field measurements were only performed for these LED arrays). NFGM were realized at $I_F = 3$ mA/LED and $I_F = 10$ mA/LED, and by linear fitting an equation was obtained for each LED array. To determine the radiant flux for a single LED at intermediate currents, Eq. S14 was used for the CC-8mm array, and Eq. S15 was used for the MC-8mm array.

$$\Phi_0 = 0.8176 I_F \quad (\text{S } 14)$$

$$\Phi_0 = 0.7839 I_F \quad (\text{S } 15)$$

In the following we highlight the modeling of the absolute irradiance for the CC-8mm array at $I_F = 3$ mA/LED. In the model (NFGM) the irradiance distributions were obtained using Eq. S12 and the coefficients listed in Table S4. In the model (DS) the irradiance distribution was obtained from the manufacturer datasheet. The simulated irradiance of the first LED row of the CC-8mm array was compared with the irradiance extracted from ray tracing at distances ranging from 0.1 cm to 4 cm (see Fig. S5.1). For close distances ($D = 0.1$ cm, 0.5 cm, and 1 cm) the emission of individual LEDs is represented by the recurring peaks, which subside at $D = 2$ cm where the irradiance distribution becomes homogeneous. The irradiance profile obtained with ray tracing from the NFGM experiment shows an offset after $x = 7$ cm in comparison with the models, which is explained by a slight misalignment of the LED board during near-field measurements. Nevertheless, the irradiance profiles can be compared for $x < 7$ cm, and it is found that the model (NFGM) is able to predict both the magnitude and the distribution of irradiance for all distances.

On the other hand, the model (DS) overestimates the magnitude of irradiance two-fold at $D = 0.1$ cm. The error in irradiance magnitude decreases at $D = 0.5$ cm, but the model (DS) indicates a less homogeneous irradiance distribution compared with NFGM. For $D = 1$ -2 cm, the model (DS) performs better, however it tends to underestimate the irradiance which becomes apparent above 2.5 cm (see Fig. S5.1e-h).

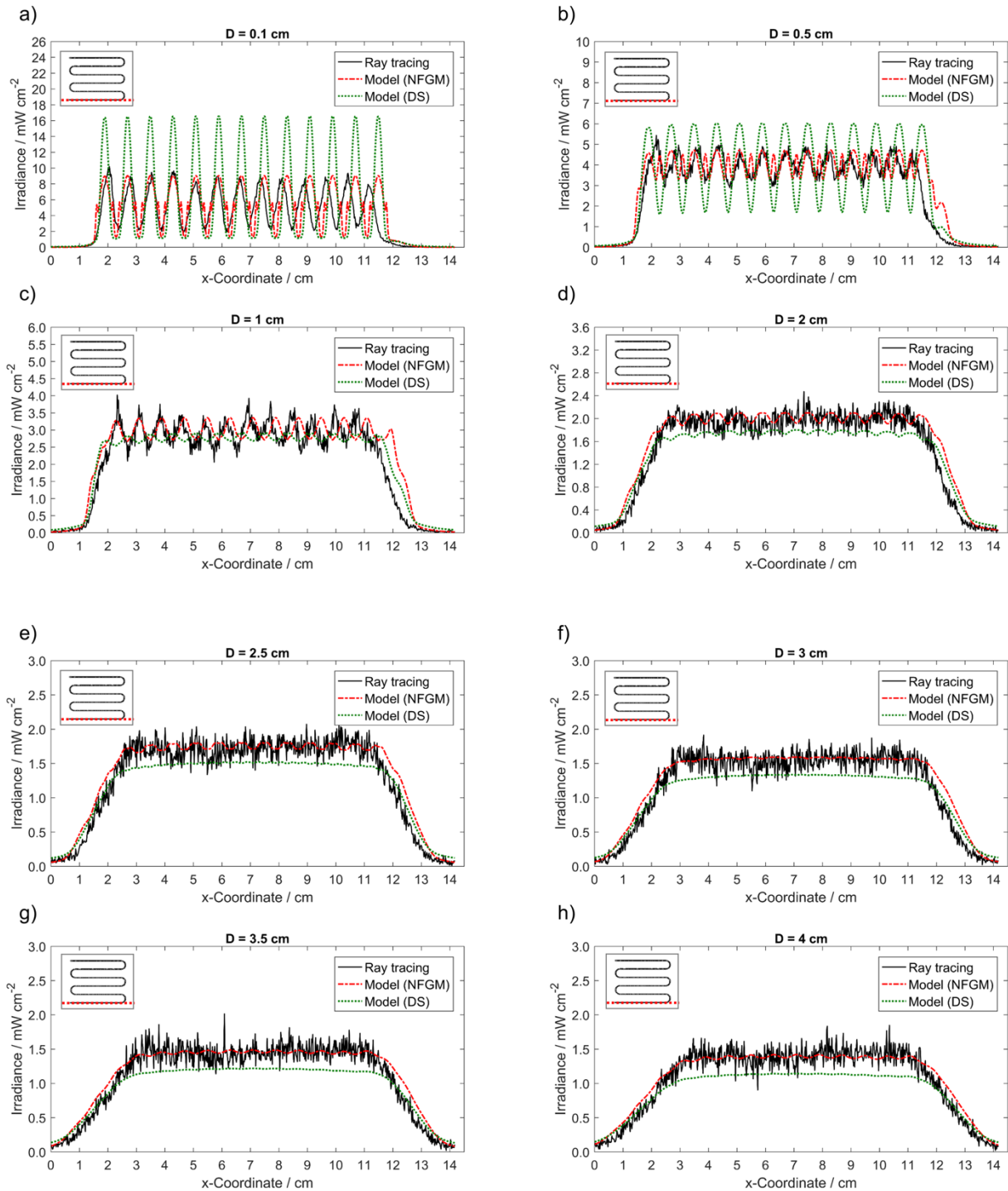


Figure S5.1. Comparison between the irradiance for CC-8mm extracted from ray tracing and predicted using model (NFGM) and model (DS). The comparison is realized for the first row of the LED array as shown in the inset at a) $D = 0.1$ cm, b) $D = 0.5$ cm, c) $D = 1$ cm, d) $D = 2$ cm, e) $D = 2.5$ cm, f) $D = 3$ cm, g) $D = 3.5$ cm, h) $D = 4$ cm and for a forward current of $I_F = 3$ mA/LED.

The lower irradiance predicted by the model (DS) at larger distances was attributed to the emission at large angles which is not present in the angular distributions obtained from NFGM (see Fig. S5.2). This was proven by simulating the irradiance using an irradiance distribution where the normalized irradiance at angles larger than 45° is set to zero (DS modified). As it is showed in Fig. S5.3a-d, the prediction of the model (DS modified) is now similar to the predictions of the model (NFGM). Therefore, even if the contribution of large angles was very small ($E < 0.05$), the effect on the absolute irradiance was significant. Therefore, when working with multiple LEDs, the resulting irradiance on a parallel plane is not intuitive and modeling tools with correct radiation pattern should be used.

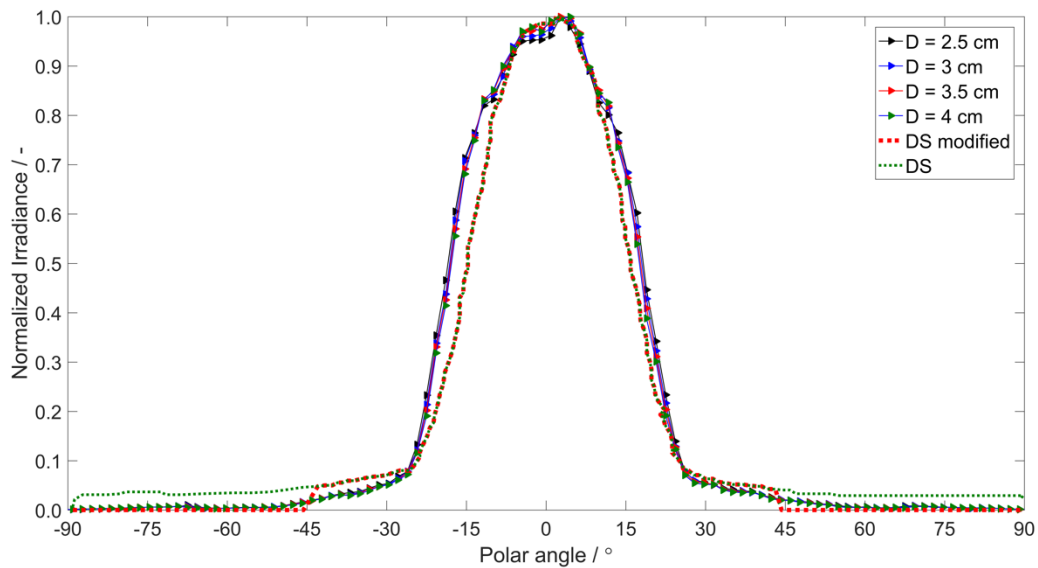


Figure S5.2. Variation of the normalized irradiance as a function of the polar angle, θ , at different distances, D , extracted from NFGM. DS denotes the normalized irradiance distribution extracted from the manufacturer datasheet, representing the far-field region. DS modified represents the DS irradiance distribution in which the irradiance for $\theta > 45^\circ$ is set to zero.

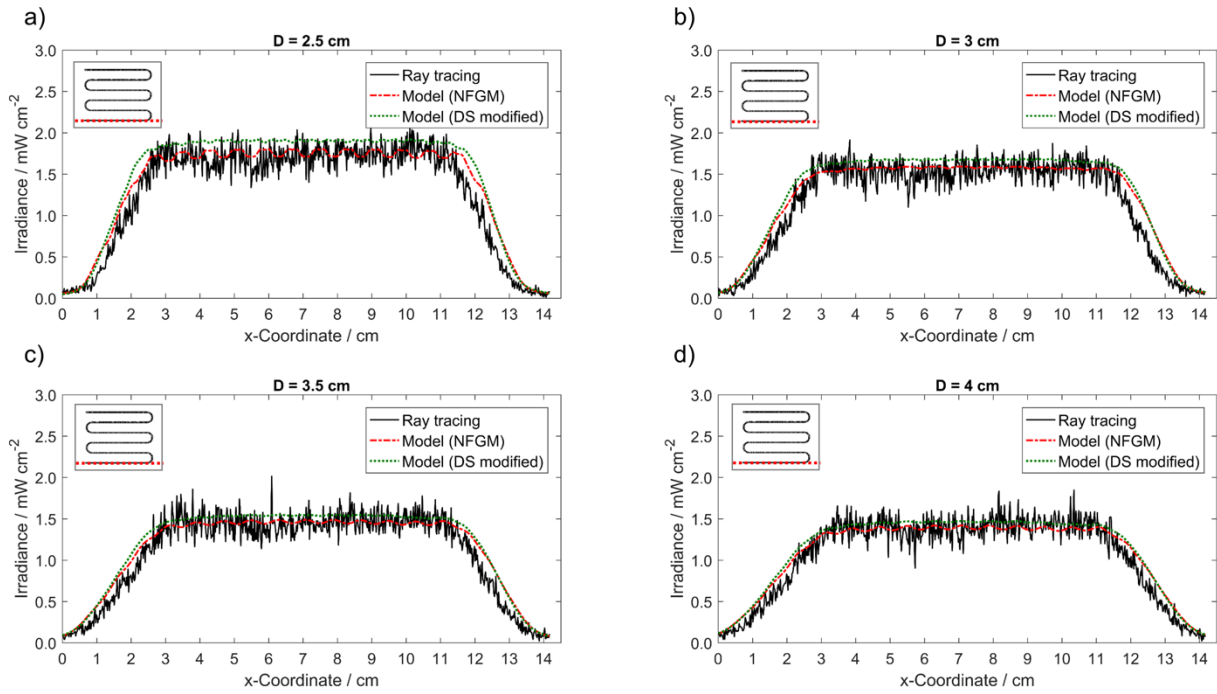


Figure S5.3. Comparison between the irradiance for CC-8mm extracted with ray tracing from the NFGM and predicted using model (NFGM) and model (DS modified). The comparison is realized for the first row of the LED array as shown in the inset and at a) $D = 2.5$ cm, b) $D = 3$ cm, c) $D = 3.5$ cm, d) $D = 4$ cm and for a forward current of $I_F = 3$ mA/LED.

S6. Optical properties of LEDs

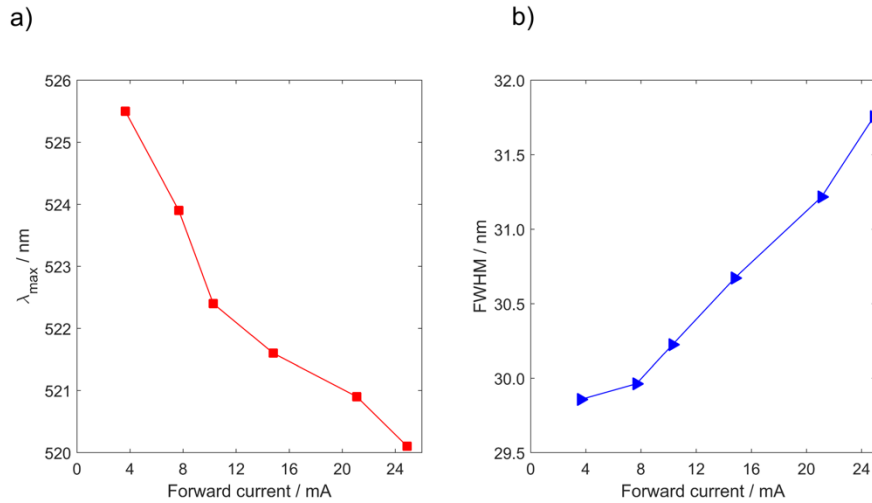


Figure S6. a) Variation of the maximum emission wavelength, λ_{\max} , in function of the forward current, I_F . b) Variation of the FWHM in function of forward current, I_F .

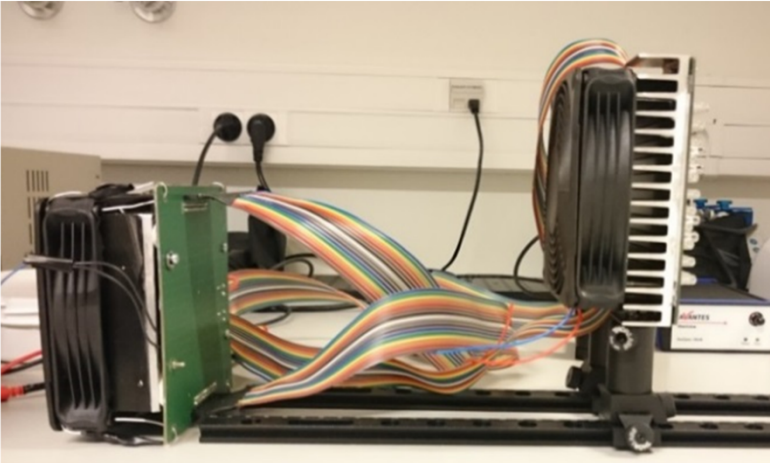
S7. Design and operation of the LED and driving boards

The role of the driving board is to maintain a similar forward current through the LEDs placed on the board. However, as LEDs from different groups (LED1, LED2, LED3) experience different forward voltages at the same forward current, they consume a different power resulting in different heat generation. This difference is limited when the LEDs are driven at small currents, as is the case in our study. However, the presence of potential hot spots on the LED boards were avoided by (i) not including LEDs from groups 2 and 3 and (ii) by an efficient cooling of the LEDs. The connection between the driving board and the LED array is realized through a ribbon cable with a standard connector (see Fig. S7.1a). Therefore, the driving board can be used with any of the designed LED arrays. Figure S7.1b illustrates the layout of the driving board which is a transistor-based circuit with a current mirror topology. It can control the current through up to 28 LED series. The driving board is necessary not only when the electrical characteristics of the LEDs are different as discussed in the manuscript, but also when the series of LEDs do not contain the same number of LEDs (see Table S7). For example, driving the MC-8mm array involves driving series of 6 LEDs and 7 LEDs respectively. Without a driving board the current will pass mainly through the series with 6 LEDs due to its lower total resistance. Moreover, for a stable current, the transistors should be operated under isothermal conditions. For this reason, a viscous thermoconductive paste (Computer-Systems, K5 PRO) was applied on the transistor surfaces enabling good contact with a heat sink (Aavid Thermalloy, thermal resistance 0.72K/W). A DC axial fan (ebm-papst, 8 W) was used to dissipate the heat produced by the driving board.

Table S7. LED series in the designed LED boards.

LED board, $s = 8 \text{ mm}$	LED board, $s = 6.5 \text{ mm}$
<ul style="list-style-type: none">• 12 series of 7 LEDs• 10 series of 6 LEDs	<ul style="list-style-type: none">• 19 series of 7 LEDs• 5 series of 8 LEDs• 1 series of 4 LEDs

a)



b)

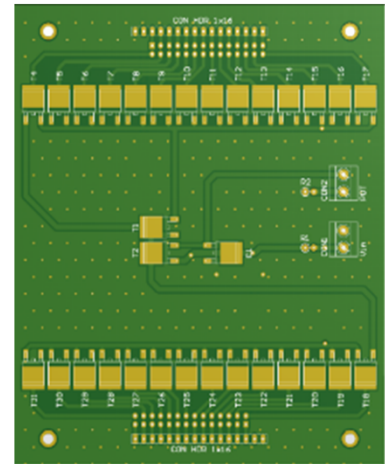


Figure S7.1. a) Photo of the LED and driving boards equipped with heat sinks and fans. b) Circuit layout of the driving board. The yellow squares represent the transistors.

The driving board is powered by a lab power supply (Velleman). The voltage of the power supply is set at 25 V irrespective of the LED array. A variable resistor made in-house is connected to the driving board for controlling the forward current through the LEDs. The variable resistor involves 2 modules with relays (Yoctopuce) and resistors, and is controlled via 2 USB cables from a computer (see Fig. 1 in the manuscript). The procedure for building a variable resistor is available online: <http://www.yoctopuce.com/EN/article/building-a-usb-driven-variable-resistor>.

The working principle is based on the fact that the current is controlled by the resistance value of the variable resistor; when the resistance changes, the current through the LEDs will change as well. This is realized by connecting resistors in series, and relays in parallel with the resistors. By switching on a relay, the resistor connected in parallel with the relay will be by-passed, and the current will increase accordingly. As shown in Fig. S7.2 multiple resistors were soldered in series to achieve the desired resistances (e.g. 40 Ω was obtained by connecting 2 resistors of 20 Ω). The relays are switched ON and OFF by a script written in Python using the Command Prompt environment. In the Command Prompt environment, the value of the desired resistance is entered, determining a certain value of the forward current through the LED series. The resolution of the current control using the variable resistor is around 0.2 mA. The obtained forward current through a selected LED series is monitored using a digital multimeter. We observed that a change in the operating conditions of the light source (e.g. variation of the ambient temperature) results in a change in the current obtained for the same resistor setting. Therefore, the results of the experiments are always compared at the same current, not at the same resistor setting.

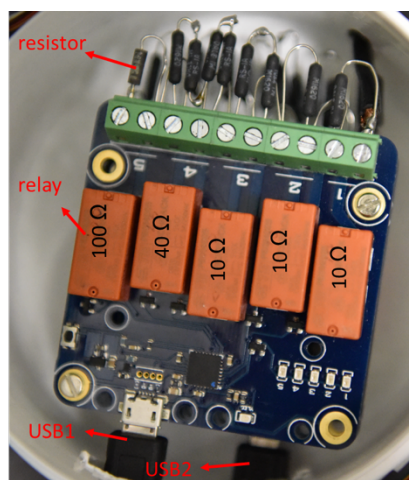


Figure S7.2. Photo of the variable resistor.

S8. Calculation of the STY

In this work, the space-time yield STY [$\text{mol L}^{-1} \text{s}^{-1}$] was assumed equal to the averaged photoreaction rate in the reactor which can be calculated as¹:

$$\text{STY} = \bar{R} = \phi_{\text{avg}} \frac{I_{\text{abs}}}{V} \quad (\text{S } 16)$$

where ϕ_{avg} is the averaged quantum yield which is equal to $0.02 \text{ mol Einstein}^{-1}$ at $I_F = 8 \text{ mA/LED}$ and I_{abs} is the photon flux absorbed by the DAE CF solution.

The absorbed photon flux, I_{abs} , can be expressed as a function of the received photon flux as:

$$I_{\text{abs}} = I_0 \left(1 - 10^{-\varepsilon_{\text{avg}} c l_{\text{avg}}} \right) \quad (\text{S } 17)$$

As the absorbed photon flux, I_{abs} , depends on the concentration of DAE CF, the reaction rate is calculated for a case where all the photons received in the channel are absorbed (I_{abs} is equal to I_0). Therefore, the averaged reaction rate can be expressed as:

$$\bar{R} = \phi_{\text{avg}} \frac{I_0}{V} \quad (\text{S } 18)$$

References

1. A. Roibu, S. Fransen, M. E. Leblebici, G. Meir, T. Van Gerven and S. Kuhn, *Sci. Rep.*, 2018, **8**, 5421.